Revised version #2

Experimental vs. natural fulgurite: a comparison and implications for the formation process

A. Zeynep Çalışkanoğlu[a,*], Corrado Cimarelli[a], Donald B. Dingwell[a], Alessandra S. B. Camara[b]

[a]Department of Earth and Environmental Sciences, Ludwig-Maximilians-Universität, Theresienstraße 41, 80333 Munich, Germany

[b]Institute of Energy Systems Munich, Universität der Bundeswehr, Werner-Heisenberg-Weg 39, 85577 Neubiberg, Germany

*Corresponding author's E-mail address: zeynep.caliskanoglu@min.uni-muenchen.de

Abstract

Fulgurites are glassy structures formed when lightning strikes the ground, causing ground material (e.g., rocks, sediments, or soil) to melt and fuse. While fulgurites are relatively rare, they provide valuable insights into paleoecology and may play a key role in prebiotic chemistry. Despite their significance in nature, understanding the conditions underlying the formation of fulgurites poses severe challenges, as the physical parameters and timing of the fulgurite-generating lightning event still need to be discovered.

Here, we use a unique opportunity from the recent *in situ* discovery of a natural fulgurite still embedded in its protolith. Using a high voltage setup, we further compare this natural fulgurite with the experimentally generated fulgurite obtained from the original protolith. The natural and experimental fulgurites exhibit evidence of similar melting sequences and post-

melting recrystallization structures. Using Raman spectroscopy applied to the quartz phase transition, we estimate the thermal gradient present in the fulgurite during formation to be a minimum of 1600°C at the inner wall of the fulgurite and ca. 600°C at the outer wall of the fulgurite. The natural fulgurite-generating event is also accessible via World Wide Lightning Network data. Those findings suggest that the current responsible for the cloud-to-ground lightning discharges that generated the natural fulgurite lay in the range of 11.960 kA to 14.473 kA. The state of the experimental fulgurites matched that of the natural fulgurite, validating the experimental option for studying fulgurite generation.

Keywords: Fulgurite, Lightning discharge, Experiment, WWLLN, ENTLN

INTRODUCTION

Fulgurites are irregular, glassy, tube-shaped formations that occur when lightning discharges (specifically cloud-to-ground or CG) melt the Earth´s surface at peak temperatures, followed by rapid cooling. They typically contain a large glass fraction hosting some initial unmelted lithologies and often exhibit some quench crystallization.

Only one-third of thundercloud lightning discharges are estimated to reach the ground, potentially generating fulgurites (Rakov 2016). Despite the limited number of examples, it has been proposed that fulgurites may offer valuable data for paleoecology reconstructions (Navarro-González et al., 2007; Ballhaus et al., 2017) and demonstrate the existence of rare essential prebiotic chemical reactants, such as phosphite (e.g., Pasek and Block, 2009; Hess et al., 2021; Çalışkanoğlu et al., 2023a; Bindi et al., 2023).

Previous fulgurite research has predominantly focused on natural examples (e.g., Pasek et al., 2012; Ende et al., 2012; Stefeno et al., 2020; Karadag et al., 2022), with very few experimental studies to date (e.g., Castro et al., 2020; Genareau et al., 2017). Those pioneering experimental studies were severely limited in their ability to mimic natural lightning due to constraints arising from technical aspects of the experiments, such as the absence of a trigger or a continuing current. They, therefore, largely fail to replicate accurately the conditions of fulgurite petrogenesis. In contrast, the high current and voltage experimental setup (see detail in Çalışkanoğlu et al., 2023b) employed here enables the accurate simulation of lightning discharges responsible for fulgurite formation.

Here, we compare a natural fulgurite (Eastern Türkiye) and an equivalent experimentally generated fulgurite obtained using the *in situ* adjacent protolith as a starting material. The experimental fulgurite, generated under variable well-controlled experimental conditions, yields new insights into the textural evolution of the natural fulgurite and about temperature gradients during melting and recrystallization at high cooling rates. Simultaneously, we report

the first detailed measurements of lightning discharge parameters that we infer led to the formation of the natural fulgurite, thereby effectively constraining the electrical conditions necessary for fulgurite formation.

MATERIAL AND METHODS

The natural fulgurite

A sample of natural fulgurite and its adjacent protolith were obtained from a private seller who discovered the fulgurite in north-west Van-Türkiye (38°13'17.6"N 44°15'55.9"E) in mid-April 2021 (Fig. 1a,b) after a thunderstorm of April 1st, 2021. The investigated natural fulgurite part will be detailed in the Result section. The CG lightning associated with that thunderstorm has been detected by radio-frequency antennas of Earth Networks Total Lightning Network (ENTLN; Zhu et al., 2022). In addition to the approximate location of the lightning discharge, the antennas provide the magnitude of the current associated with each lightning event. This discovery provides us with a unique opportunity to evaluate natural fulgurite formation versus experimental fulgurite formation from the protolith using independent control of lightning parameters under realistic conditions.

The target (protolith) material

The protolith (a soil-bearing epiclastic sediment), collected from an area immediately adjacent to the natural fulgurite (Fig. 1a), was used as a target material for the fulgurite synthesis experiments. The remote location means no nearby communication poles might have accidentally generated the fulgurites “artificially” (e.g., Kassi et al., 2013).

The local geology consists of several geological units from oldest to youngest: 1) pre-Neogene pyroclastic deposits (pumice, tuff, and ignimbrites) and intermediate (andesite/trachyandesite) deposits from Mount Yiğit (Türkecan 2017), 2) Neogene clastic

rocks (conglomerate, sandstone, marl, and - locally - tuff and lava blocks), 3) Pliocene sedimentary deposits (Şenel et al., 1984) and basaltic lava flows, which represent the latest stage of Mount Yiğit volcanism (1.87 ± 0.07 My; Allen et al., 2011). The protolith used as experimental target material was collected from where the Neogene clastic rocks crop out (Fig. 2a).

The protolith appears yellowish-brown and is composed of rock fragments of varying sizes, ranging from ca. 30 μm to a few centimeters, consisting of mono- and polymineralic grains. The rock fragments exhibit sub-rounded to rounded edges. Energy-dispersive X-ray spectroscopy (EDS) analysis reveals that the monomineralic grains include quartz, plagioclase, and alkali feldspar, along with minor Fe- and Ti-oxides (Fig. 2b,c,d). The polymineralic grains exhibit diverse compositions, but plagioclase, quartz, and alkali feldspar are the most common minerals, with minor hornblende, biotite, apatite, zircon, Fe- and Ti-oxides (Fig. 2d,e). Most clasts are fully crystalline (Fig. 2e-g), but some exhibit up to 20% glass (Fig. 2h). Backscattered Electron (BSE) images reveal no evidence of lightning-induced effects in the protolith used subsequently as experimental target material.

Sample preparation and analytical techniques

The target material was thoroughly cleaned to remove any potential macroscopic organics (plants). The most comprehensive possible range of macroscopically distinct clasts was selected and roughly crushed to less than 10 mm, and a mixture of them was embedded in epoxy for further analytical analyses.

Several 10 mm chips of fulgurites (both natural and experimental) were embedded in their respective epoxy mounts for microtextural analyses.

The surfaces of further chips of both natural and experimental fulgurites were examined using a Keyence 3D Laser Scanning Confocal Microscope (LSCM) VK-X1000 with a 5x

objective lens (WD 22.5) in the Department of Earth and Environmental Sciences at Ludwig-Maximilians-Universität (LMU), Munich - Germany.

BSE images of the target material, natural and experimental fulgurite samples, were collected using Scanning Electron Microscopy (SEM) at LMU - Munich with an accelerating voltage of 20 kV under a low vacuum. Semi-quantitative chemical composition data collection at the SEM was conducted through EDS using an Oxford Instrument Aztech software (AztechEnergy Advanced EDS-System) on the natural fulgurite, its protolith, and the experimental fulgurite.

We used the confocal HORIBA Jobin Yvon XploRa micro-Raman spectrometer at the Mineralogical State Collection Munich (SNSB) to identify mineral phases. The instrument was calibrated with a silica standard, and the spectra were acquired with a green Nd: YAG-Laser (532 nm wavelength), focused through the 100LWD objective lens, with 0.9 μm laser spot diameter. Grating of 1800T, a confocal hole of 300 μm, a slit of 100 μm, and an exposure time of 30 s three times acquired were applied. The backscattered Raman radiation was collected between 100 - 1500 cm^{-1}, with an error of ±1.5 cm^{-1}, to include the low and high wavenumber regions.

Fulgurite synthesis experiments

We simulated natural lightning discharges in the high voltage laboratory at Universität der Bundeswehr (UniBw) in Germany, utilizing a DC source with a trigger-pulse setup to synthesize a fulgurite. The setup was designed based on recommendations from the lightning research community, such as the waveforms specified in IEC 62305 (International Electrotechnical Commission [IEC] 2010) derived from studies of natural lightning phenomena. For further details regarding the experimental methodology and schematic diagram of the setup, please refer to Çalışkanoğlu et al. (2023b).

The lightning strikes are conducted between two electrodes placed inside a cylindrical sample container, which is connected to an electrical apparatus consisting of two parts: a Marx generator (which produced the trigger pulse) and a DC source (which acted as a prolonged current generator). The container was filled with approximately 250 g of target material. Initially, the Marx generator generated ca. 135 kA for ca. 100 microseconds, creating a conductive path between the electrodes, which were 5.7 cm apart. This high voltage and current initiated the melting of the target material. Subsequently, the DC source was kept constant between ca. 280 and ca. 320 A for ca. 500 milliseconds, simulating the long duration of a natural lightning discharge (Rakov and Uman, 2003; Lapierre et al., 2014). This prolonged current promoted the melting of more material and facilitated the formation of a fulguritic mass.

Several experimental trials were conducted to establish the setup conditions and comprehend the material's behavior under high current and voltage conditions. All experiments were carried out at atmospheric temperature and pressure. In the first experiment, the target material was utilized in its natural form (fragments ranging from 32 μm to a few cm), but no melted pieces or fulguritic structures were observed. Simulated lightning is characterized by a lower peak current than natural lightning, thus preventing larger grains from melting. To ameliorate this discrepancy, ca. 50% of the coarse fraction (> 10 mm) was removed, and the experiment was repeated under the same electrical parameters as above, resulting in the formation of a fulgurite. The waveform of the experimental current was recorded using a Measurement Impulse Analyzer System (MIAS) at an 800-1000 ms time interval.

Field lightning monitoring

ENTLN comprises more than 1800 sensors deployed across more than 100 countries, which detect broad-spectrum electric field signals originating from intracloud (IC) and CG lightning events (Liu and Heckman, 2011). The CG lightning data is obtained from the World Wide

Lightning Location Network (WWLLN) to enhance ENTLN detection capabilities. The WWLLN detects, locates, and timestamps lightning strikes worldwide with a spatial accuracy of 10 km and a temporal accuracy of 10 μs (Abreu et al., 2010; Holzworth et al., 2019; Hutchins et al., 2012, 2013; Rodger et al., 2004, 2005). We utilized WWLLN data to identify natural lightning events, which might have generated our natural fulgurite.

We focused on the period of April 1-15, 2021. Our search area was limited to an 8 km radius around the location where the natural fulgurite was found. We detected one IC and two CG lightning events (CG-1 and -2) within the focused area and time frame by using ENTLN data (Table 1 and Fig. 1a). IC events do not generate fulgurite; thus, the IC data is neglected in the present study. Both CG-1 and CG-2 lightning strokes showed a "downward negative" direction (the most common for global CG lightning, Rakov and Uman (2003)). The CGs were ordered according to the time of occurrence, with the location estimates CG-1 and CG-2 illustrated in Fig. 1a. It should be noted that due to the technical limitations of the antenna network, the designated locations of the CGs are, within error, equivalent to the fulgurite location (i.e., WWLLN - Rodger et al. (2005); ENTLN - Zhu et al. (2022)). Considering the data from the WWLLN, we propose that one of these occurrences generated the investigated natural fulgurite.

RESULTS

Natural fulgurite

The natural fulgurite is ca. 112 cm long and ca. 105 cm wide (Fig. 1b). It displays several small branches connected to two main branches. An available piece of this fulgurite was obtained commercially and investigated in the present study (Fig. 3a,b). Hereafter, we refer to this sample as the "natural fulgurite". The natural fulgurite is ca. 17 cm in length and has a diameter of ca. 6 cm. It appears darker than the protolith. The outer surface of the natural

fulgurite has a rough texture with several unmelted grains remaining from the protolith (Fig. 2a). In contrast, the central portion of the natural fulgurite is entirely glassy. Vesicles of variable shapes and sizes are present. The "main void" is the largest vesicle (ca. 2.5 cm in size) in the natural fulgurite, as shown in Fig. 3b. Immediately adjacent to the glassy region is a zone of large vesicle concentration. Smaller vesicles are distributed from the glassy region to the unmelted protolith. (Fig. 3c). The fulgurite wall thickness varies from ca. 1 cm to 3 cm. The fulgurite contains unmelted to partially-melted, angular, and sub-angular grains (up to a few millimeters) and a fully-melted glassy region. Unmelted grains are common on the outer wall of the fulgurite, whereas partially melted grains are typically scattered in the glassy mass. BSE images show no sharp transition between unmelted and partially-melted grains. The glassy mass is composed of a heterogeneous mingling of molten materials (Fig. 3d).

Natural fulgurite grains are mono- and polymineralic, occurring in unmelted and partially-melted states. Monomineralic grains are typically alkali feldspar, plagioclase, and quartz or minor Fe- and Ti-oxides. Melts apparently derived from feldspar mingle with the matrix-derived melts, as evidenced by heterogeneity in the glass, in the form of flow structures (Fig. 3d). Partially-melted quartz crystals are commonly fractured (Fig. 3e). The phase change from alpha (α) quartz (crystals located in the outer zone of the fulgurite) to cristobalite (crystals located close to the inner wall) was also detected.

Post-melting recrystallization structures with different compositions were detected, as shown in Table 2. No orientation is apparent in the growth pattern of these structures. Their size reaches a maximum of 1 mm. Prismatic-tabular structures are observed, which are enriched in SiO_2, Al_2O_3, CaO, and Na_2O (Fig. 3f). Skeletal structures are observed, which are enriched in MgO (Fig. 3g). Other structures (i.e., cross, spherical and another skeletal) have notably high FeO contents (Fig. 4a-c). The cross and spherical structures are found in proximity to one another and appear to be formed sequentially. These structures' considerably smaller size (<1

μm) prevents accurate composition measurements because of SiO_2 and Al_2O_3 contamination from the surrounding material. However, their compositions appear similar to those of the Fe-containing phases.

The polymineralic grains in the natural fulgurite consist mainly of quartz, plagioclase, and alkali feldspar, with minor biotite, hornblende, apatite, zircon, and oxides (Fe and Ti). These grains are found in both unmelted and partially-melted regions. The volume fraction of unmelted grains is much lower than that of partially-melted grains in the glassy region. Feldspar crystals exhibit three morphologies: "solid," "vesiculated", and "molten". The solid morphology represents the feldspar crystals (either alkali feldspar or plagioclase) that do not show any chemical and physical changes (i.e., unmelted) (Fig. 4d). These crystals are only found in the outer wall of the natural fulgurite. The vesiculated morphology indicates crystals containing mainly rounded vesicles (Fig. 4e). They are mostly found in the middle of the natural fulgurite wall. The chemical composition of this region is enriched in SiO_2, Al_2O_3, Na_2O, and K_2O. The Na_2O and K_2O values are variable depending on the volume ratio of plagioclase and alkali feldspar in the primary grains. The molten morphology may result from feldspar crystals melting completely in the presence of some other minor phases, such as Fe-oxide (Fig. 4f).

Experimental fulgurite

The experimentally-generated fulgurite is also tube-like without branches (Fig. 5a) and appears dark brown. It is approximately 7 cm in length and 1 cm in width, with a main void diameter of approximately 7 mm (Fig. 5b). The thickness of the fulgurite wall is ca. 2 mm. The distribution of unmelted and partially-melted grains, as well as the glassy region, is found to be quite similar to that of the natural fulgurite, and there is no sharp transition between unmelted and partially-melted grains at the outer edge of the experimental fulgurite. However,

the proportion of the unmelted grains in the glassy region is much lower than in the natural fulgurite, presumably due to the finer grain size of the target material. The average grain size of both the unmelted and partially-melted grains is approximately 0.5 mm. Several vesicles, ranging up to 1 mm in size (rounded and sub-rounded), are highly concentrated between unmelted and partially-melted regions (Fig. 5c).

The experimental fulgurite contains mono- and polymineralic grains in both unmelted and partially-melted forms. Quartz and feldspar crystals are the two monomineralic grains. Feldspar crystals are mingled in the glassy region, resulting in the flow structures observed (Fig. 5d). Quartz crystals are ca. 0.5 mm in size (Fig. 5e), and they exhibit physical deformation such as fractures (Fig.5f) and have been identified as α-quartz via Raman spectroscopic analysis.

Three distinct post-melting recrystallization structures are observed. They are numbered 1, 2, and 3 based on their structural differences from right to left on a BSE image (Fig. 5g). They exhibit strong FeO enrichment together with high SiO_2 and Al_2O_3 contents (Table 3). Structure 1 displays a cross-formed shape, as observed in the natural fulgurite (Fig. 4a). In structure 2, radial arms extend from a central point to form spherulites. Structure 3 displays a symmetric skeletal form. The structures 1 and 3 cover a larger area of the fulgurite than the structure 2. Analysis of these small Fe-rich suffers from contamination (i.e., SiO_2 and Al_2O_3) originating from the surrounding glass.

The polymineralic grains consist mainly of quartz, plagioclase, and alkali feldspar. Hornblende, apatite, and minor Fe and Ti. These minor phases are solely detected in the partially melted grains near the outer wall of the experimental fulgurite. Quartz crystals have retained their general form with numerous fractures and show no notable chemical changes. In contrast, feldspars exhibit chemical and mechanical changes. They show the same textural morphologies (solid, vesiculated, molten) (Fig. 5h-j) as described for the natural fulgurite (Fig.

4d-f). Feldspar crystals (alkali feldspar and plagioclase) in the solid morphology are detected in the outer wall of the experimental fulgurite (Fig. 5h). They exhibit enhanced vesiculation (Fig. 5i). In the molten morphology, feldspars appear entirely molten without any recognizable morphological crystal form close to the interior fulgurite wall, and they are surrounded by fractured quartz crystals (Fig. 5j). EDS measurements on the well-mixed glassy region indicate that the glass composition of the experimental fulgurite is quite similar to that of the natural fulgurite (Table 2).

DISCUSSION

Fulgurite was experimentally generated from the protolith recovered adjacent to a natural fulgurite. The formation of a fulgurite is confirmed to be a complex process that depends on several factors, including the lightning parameters (i.e., temperature and current), as well as the composition and the state of the host rock. Even though the current intensities of the natural lightning discharge, ca. 13.000 kA ± 1.250 (Table 1), and the experiment, ca. 300 A are vastly different, our results reveal that the fulgurites generated in nature and experiments resemble each other closely. A notable exception is that the higher natural current does lead to a higher degree of melting of coarser grains. A possible explanation for this scale-invariant character may lie in the intrinsic fractal nature of lightning discharges (Niemayer et al., 1984; Wiesmann and Zeller, 1986). Previous work from Çalışkanoğlu et al. (2023b) indicates that the continuing current of a lightning strike has a noticeable effect on the formation of fulgurite, indicating a threshold of ca. 100 ms for fulgurite formation. We confirm here that a 300 A current and a prolonged duration of discharge (ca. 100 ms) facilitates the formation of fulgurite from the silicate protolith (Maurer 2021), as it has been previously demonstrated for non-silicate (Çalışkanoğlu et al. 2023a) protolith.

Temperature gradients and grain size distribution both exert first-order influences on fulgurite texture. The temperature of natural lightning discharges typically ranges between 10.000 to 28.000 K (Paxton et al., 1986). Based on melting temperatures, we observe that our simulated lightning discharge generates a minimum of ca. 2000 K (Çalışkanoğlu et al., 2023a-b). Regions experiencing lower temperatures, due to their distal location to the lightning plasma and higher concentration of coarse grain sizes, exhibit a higher proportion of partially-melted and unmelted grains in the fulgurite, yielding distinct regions whose textures are systematically defined by their degrees of melting (e.g., Hess et al., 2021; Kenny and Pasek, 2021; Çalışkanoğlu et al., 2023a-b). In both nature and experiment, coarse grains that have been partially melted exhibit distinctive flow structures in their glassy products, indicating that such melts are not homogenized during fulgurite formation (c.f. Lavallée et al., 2015). In contrast, the homogeneous glassy (fully remelted) regions of experimental and natural fulgurites exhibit similar chemistry as determined by SEM/EDS (Table 2).

Quartz crystals (initially both mono- and polymineralic grains) undergo a phase change (Fig. 6a,b) with increasing temperature, resulting in a fractured structure. Folstad et al. (2023) indicate that cracks in quartz are commonly observed in two temperature ranges. The first range, approximately 300-600°C, primarily arises from volume changes in impurity regions, uneven surfaces of quartz, and/or the presence of fluid inclusions. The second range, ca. 1300-1600°C, is likely a consequence of the phase transformation of quartz from β-quartz to β-cristobalite. As noted above, the natural fulgurite exhibits α-quartz in the outer wall and β-cristobalite in the inner wall. This implies the presence of a strong temperature gradient across ca. 1 cm. In contrast, the experimental fulgurite exhibits no cristobalite. Possible reasons for this discrepancy include (1) the simulated lightning may not have reached the equivalent temperature range and/or (2) the pressure generated by simulated lightning may be lower.

Feldspar crystals situated in proximity to the lightning plasma undergo complete melting, whereas those subjected to lower temperatures display partial melting with vesicle formation. This distinction within the feldspar crystals supports the strong temperature gradient extending from the inner wall (adjacent to the plasma) to the outer wall of the fulgurite.

Upon cooling, both the natural and experimental fulgurites reveal the presence of multiple coexisting crystalline structures (i.e., spherical and dendritic) (Fig. 3f-g, 4a-c and 5g). Similar crystal structures have also been reported in other rapidly quenched glasses, such as impactites, meteorites, and chondrules (e.g., Kumler and Day, 2021). Skeletal structure (magnetite) has previously been documented in fulgurites by Ablesimov et al. (1986) and Grapes and Müller-Sigmund (2010). To the best of our knowledge, this study marks the first documented occurrence of spherical Fe-rich forms within natural and experimental fulgurites. The juxtaposition of distinct growth patterns and crystal sizes might reflect locally varying melt compositions and/or different cooling rates determined by proximity to the lightning plasma and heterogeneous composition.

IMPLICATIONS

This work demonstrated a realistic comparison between natural and experimental fulgurites for the first time, revealing a remarkable similarity in their textural and mineralogical evolution. This validates that the state of the experimental fulgurite matched that of the natural fulgurite using the DC source trigger-pulse setup as a lightning simulator. This work also further documents the physical parameters (maximum voltage and current) of lightning strikes that likely generated the natural fulgurite. Our results interestingly suggest a scale-invariant character of the experimental fulgurites concerning the natural one, whereby the lower voltage and current values used in the experiments allow the reproduction of identical textures observed in the natural fulgurite. As shown in previous experiments, we confirm the importance of long-

duration (100's ms) continuous currents in favoring extensive melting and, ultimately, the fulgurite formation. This work introduces a novel methodology for reproducible fulgurite generation through laboratory experiments. This opens up possibilities for systematic petrogenetic analysis of fulgurite formation with broader geological implications, providing researchers with a controlled environment to explore and understand the processes involved.

ACKNOWLEDGMENTS

The research was financially supported by the Volkswagen Foundation (VW Stiftung) under Project-ID 94809. DBD acknowledges ERC 2018 ADV Grant 834255 (EAVESDROP), and CC acknowledges ERC 2019 COG Grant 864052 (VOLTA). The authors thank Dr. Jeff Lapierre for providing the ENTLN dataset. The authors thank Prof. Dr. Philippe Schmitt-Kopplin for his assistance and technical support and Prof. Dr. Daniel Weidendorfer for useful discussions and advice. They would like to thank Associated Editor Kate Kiseeva for her careful guidance and two reviewers (Christopher J. Stefano and an anonymous) for their thorough reviews.

REFERENCE CITED

Ablesimov, N.Y., Tsyurupa, A.I., and Lipatov, V.G. (1986) Phase and element ratios upon fulguritization of basalt. Trans (Dokl) USSR Acad. Scientific Earth Science Section 290, 161–164.

Abreu, S.F., Chandan, D., Holzworth, R.H., and Strong, K. (2010) A performance assessment of the World Wide Lightning Location Network (WWLLN) via comparison with the Canadian Lightning Detection Network (CLDN). Atmospheric Measurement Techniques, 3, 1143–1153, https://doi.org/10.5194/amt-3-1143-2010.

Allen, B.M., Mark, F.D., Kheirkhah, M., Barfod, D., Emami, H. M., and Saville, C. (2011) $^{40}Ar/^{39}Ar$ dating of Quaternary lavas in northwest Iran: constraints on the landscape evolution and incision rates of the Turkish–Iranian plateau. Geophysical Journal International, 1–14, https://doi.org/10.1111/j.1365-246X.2011.05022.x.

Ballhaus, C., Wirth, R., Fonseca, R.O.C., Blanchard, H., Pröl, W., Bragagni, A., Nagel, T., Schreiber, A., Dittrich, S., Thome, V. et al. (2017) Ultra-high pressure and ultra-reduced minerals in ophiolites may form by lightning strikes. Geochemical Perspectives Letters, 5, 42-46, https://doi.org/10.7185/geochemlet.1744.

Bindi, L., Feng, T., and Pasek, M.A. (2023) Routes to reduction of phosphate by high-energy events. Communication Earth & Environments, 4, 70, https://doi.org/10.1038/s43247-023-00736-2.

Castro, J.M., Keller, F., Feisel, Y., Lanari, P., Helo, C., Mueller, S.P., Schipper, C.I., and Thomas, C. (2020) Lightning-induced weathering of Cascadian volcanic peaks. Earth Planet Science Letters, 552, 116595, https://doi.org/10.1016/j.epsl.2020.116595.

Çalışkanoğlu, A.Z., Dingwell, D.B., Cimarelli, C., Camara, A.S.B., Breitzke, H., Buntkowsky, G., Pasek, M.A., Braun, D., Scheu, B., and Molaverdikhani, K. (2023a) Reactive phosphorus via simulated lightning discharge: A role for fulgurites in pre-biotic chemistry. Chemical Geology, 620, 121343, https://doi.org/10.1016/j.chemgeo.2023.121343.

Çalışkanoğlu, A.Z., Camara, A.S.B., Cimarelli, C., Dingwell, D.B., and Hess, K.U. (2023b) Experimental generation of fulgurite under realistic lightning discharge conditions. Scientific Reports, 13, 11685, https://doi.org/10.1038/s41598-023-38781-8.

Ende, M., Schorr, S., Kloess, G., Franz, A., and Tovar, M. (2012) Shocked quartz in Sahara fulgurite. European Journal of Mineralogy, 24, 499-507, https://doi.org/10.1127/0935-1221/2012/0024-2188.

383 Folstad, M.A., Yu, H., Wang, H., and Tangstad, M. (2023) Disintegration of six different
384 quartz types during heating to 1600 °C. Minerals, 13, 132, https://doi.org/10.3390/
385 min13020132.
386 Genareau, K., Gharghabi, P., Gafford, J., and Mazzola, M. (2017) The elusive evidence of
387 volcanic lightning. Scientific Reports, 7, 1–9, https://doi.org/10.1038/s41598-017-
388 15643-8.
389 Grapes, R.H., and Müller-Sigmund, H. (2010) Lightning-strike fusion of gabbro and
390 formation of magnetite-bearing fulgurite, Cornone di Blumone, Adamello, Western
391 Alps, Italy. Mineralogy and Petrology, 99, 67-74, https://doi.org/10.1007/s00710-009-
392 0100-3.
393 Hess, B.L., Piazolo, S., and Harvey, J. (2021) Lightning strikes as a major facilitator of
394 prebiotic phosphorus reduction on early Earth. Nature Communications, 12, 1535,
395 https://doi.org/10.1038/s41467-021-21849-2.
396 Holzworth, R.H., McCarthy, M.P., Brundell, J.B., Jacobson, A.R., and Rodger, C.J. (2019)
397 Global distribution of superbolts. Journal of Geophysical Research: Atmospheres, 124,
398 9996-10005, https://doi.org/10.1029/2019JD030975.
399 Hutchins, M.L., Holtzworth, R.H., Rodger, C.J., and Brundell, J.B. (2012) Far-field power of
400 lightning strokes as measured by the World Wide Lightning Location Network. Journal
401 of Atmospheric and Oceanic technology, 29, 1102-1110, https://doi.org/10.1175/jtech-
402 d-11-00174.1.
403 Hutchins, M.L., Jacobson, A.R., Holzworth, R.H., and Brundell, J.B. (2013) Azimuthal
404 dependence of VLF propagation. Journal of Geophysical Research: Space Physics, 118,
405 5808-5812, https://doi.org/10.1002/jgra.50533.
406 International Electrotechnical Commission (IEC). (2010) Protection against lightning - Part
407 1: General Principles (2nd ed.), ISBN 978-2-88912-280-6.

Karadag, A., Kaygisiz, E., Nikitin, T., Ongen, S., Ogruc Ildiz, G., Aysal, N., Yilmaz, A., and Fausto, R. (2022) Micro-Raman Spectroscopy and X-ray Diffraction Analyses of the Core and Shell Compartments of an Iron-Rich Fulgurite. Molecules, 27, 3053, https://doi.org/10.3390/molecules27103053.

Kassi, A.M., Kasi A.K., Friis, H., and Kakar, D.M. (2013) Occurrences of rock fulgurites associated with steel pylons of the overhead electric transmission line at Tor Zawar, Ziarat District and Jang Tor Ghar, Muslim Bagh, Pakistan. Turkish Journal of Earth Science, 22, 1010-19, https://doi.org/10.3906/yer-1207-6.

Kenny, G.G., and Pasek, M.A. (2021) The response of zircon to the extreme pressures and temperatures of a lightning strike. Scientific Reports, 11, 1560, https://doi.org/10.1038/s41598-021-81043-8.

Kumler, B., and Day, J.M.D. (2021) Trace element variations generated by magmatic and post-crystallization processes in eucrite meteorites. Geochimica et Cosmochimica Acta, 301, 211-229, https://doi.org/10.1016/j.gca.2021.03.002.

Lapierre, J.L., Sonnenfeld, R.G., Edens, H.E., and Stock, M. (2014) On the relationship between continuing current and positive leader growth. Journal of Geophysical Research: Atmospheres, 119, 12-479, https://doi.org/10.1002/2014JD022080.

Lavallée, Y., Hirose, T., Kendrick, J.E., Hess, K.U., and Dingwell, D.B. (2015) Fault rheology beyond frictional melting. Proceedings of the National Academy of Sciences, 112(30), 9276-9280, https://doi.org/10.1073/pnas.1413608112.

Liu, C., and Heckman, S. (2011) The application of total lightning detection and cell tracking for severe weather prediction. In Proceedings of the 91st American Meteorological Society Annual Meeting, Seattle, WA, USA, 23–27.

Maurer, B. (2021) Lightning induced olivine spherules. Experimental generation and structural and chemical characterization of crystalline and glassy particles generated by artificial lightning. [MS.c. Thesis]: Luswig-Maximilians-Universität, 71.

Navarro-González, R., Mahan, S.A., Navarro-Aceves, R., Rajot, J.L., Mckay, C.P., Coll, P., and Raulin, F. (2007) Paleoecology reconstruction from trapped gases in a fulgurite from the late Pleistocene of the Libyan Desert. Geology, 35, 171-174, https://doi.org/10.1130/G23246A.1.

Niemeyer, L., Pietrono, L. and Wiesmann H.J. (1984) Fractal dimension of dielectric breakdown, Physical Review Letters, 52(12), 1033–1036, doi:10.1103/PhysRevLett.52.1033.

Pasek, M.A., and Block, K. (2009) Lightning-induced reduction of phosphorus oxidation state. Nature Geoscience, 2, 553-556, http://dx.doi.org/10.1038/ngeo580.

Pasek, M. A., Block, K., and Pasek, V. (2012) Fulgurite morphology: a classification scheme and clues to formation. Contributions to Mineralogy and Petrology, 164, 477-492, https://doi.org/10.1007/s00410-012-0753-5.

Rakov, V.A. (2016) Fundamentals of lightning. Cambridge University Press.

Rakov, V.A., and Uman, M.A. (2003) Lightning: physics and effects. Cambridge University Press.

Paxton, A.H., Gardner, R.L., and Baker, L. (1986) Lightning return stroke: a numerical calculation of the optical radiation. Lightning Electromagnetics, 29, 2736-41.

Rodger, C.J., Brundell, J.B., Dowden, R.L., and Thomson, N.R. (2004) Location accuracy of long distance VLF lightning location network. Annales Geophysicae, 22, 747-758, https://doi.org/10.5194/angeo-22-747-2004.

454 Rodger, C.J., Brundell, J.B., and Dowden, R.L. (2005) Location accuracy of VLF World
455 Wide Lightning Location (WWLL) network: Postalgorithm upgrade. Annales
456 Geophysicae, 23, 277-290, https://doi.org/10.5194/angeo-23-277-2005.
457 Stefano, C.J., Hackney, S.A., and Kampf, A.R. (2020) The occurrence of iron silicides in a
458 fulgurite: Implications for fulgurite genesis. The Canadian Mineralogist, 58, 115-123.
459 https://doi.org/10.3749/canmin.1900019.
460 Şenel, M., Acarlar, M., Çakmakoğlu, A., Dağer, Z., Erkanol, D., Örçen, S., Taşkıran, M.A.,
461 Ünal Ulu, M.F., and Yıldırım, H. (1984) Özalp (Van)-İran sınırı arasındaki alanın
462 jeolojisi. Maden Tetkik ve Arama Genel Müdürlüğü Rapor No: 7623, Ankara,
463 (unpublished).
464 Türkecan, A. (2017) İran sınırında bir volkan – Yiğit dağı. MTA Doğal Kaynaklar ve
465 Ekonomi Bülteni, 23, 77-86.
466 Wagstaff, F.E. (1969) Crystallization and Melting Kinetics of Cristobalite. Journal of the
467 American Ceramic Society, 52(12), 650-654, https://doi.org/10.1111/j.1151-
468 2916.1969.tb16069.x.
469 Wiesmann, H.J. and Zeller, H.R. (1986) A fractal model of dielectric breakdown and pre-
470 breakdown in solid dielectrics. Journal of Applied Physics, 60 (5), 1770-1773,
471 https://doi.org/10.1063/1.337219.
472 Zhu, Y., Stock, M., Lapierre, J., and DiGangi, E. (2022) Upgrades of the Earth networks total
473 lightning network in 2021. Remote sensing, 14(9), 2209,
474 https://doi.org/10.3390/rs14092209.
475

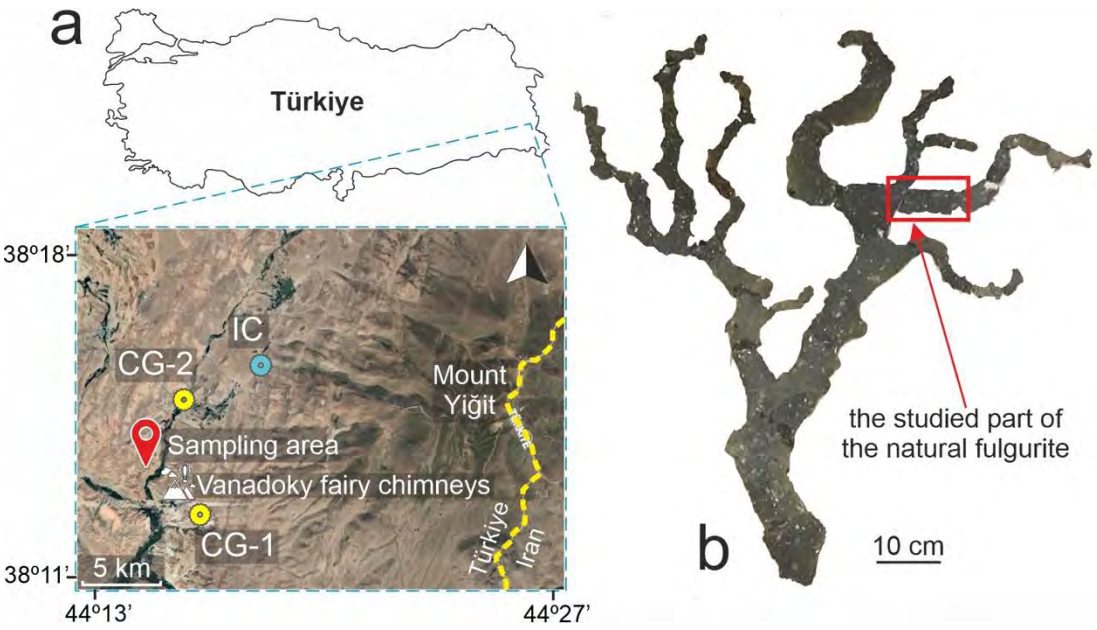

476

477 **FIGURE 1.** Sampling area and general image of the natural fulgurite. (a) The fulgurite was
478 found northwest of the Vanadoky fairy chimneys in Van, Türkiye. The ENTLN detected two
479 CG and one intracloud (IC) lightning discharges. The topographic image is taken from Google
480 Maps (2023). (b) A photographic image of the natural fulgurite is shown. The red rectangle
481 indicates the portion of the natural fulgurite object of this study.

482

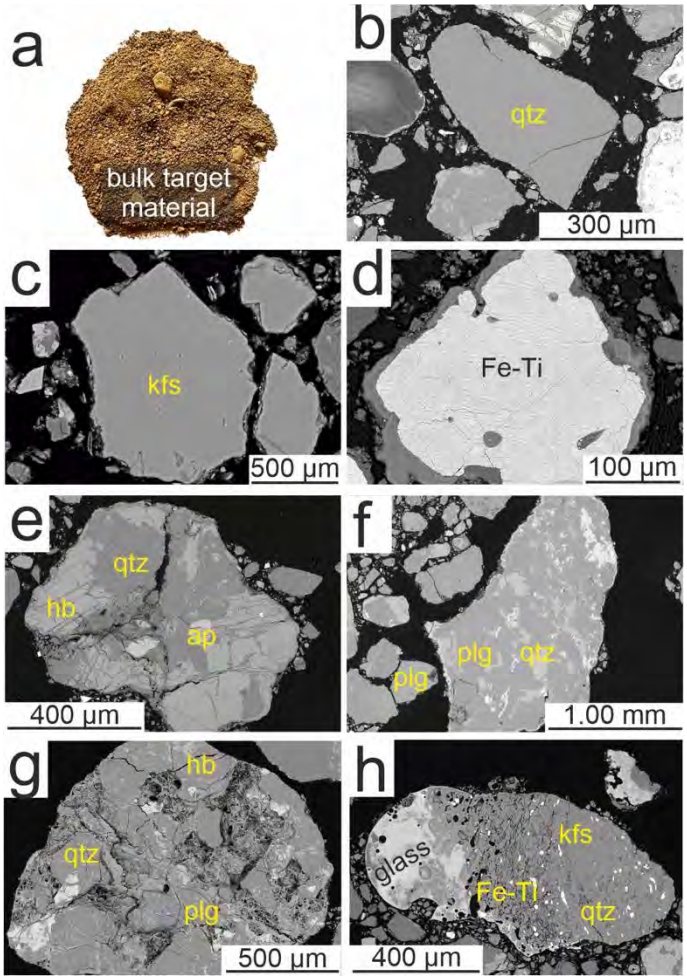

FIGURE 2. Target material and detailed BSE images of its heterogeneous grains. (a) An image of the protolith of natural fulgurite. (b-f) Mono- and polymineralic grains of the target material. These grains represent the sampling area's clastic rock unit (Şenel et al., 1984). Quartz: qtz, Alkali feldspar: kfs, Oxides: Fe-Ti, Hornblende: hbl, Apatite: ap, Plagioclase: plg.

488

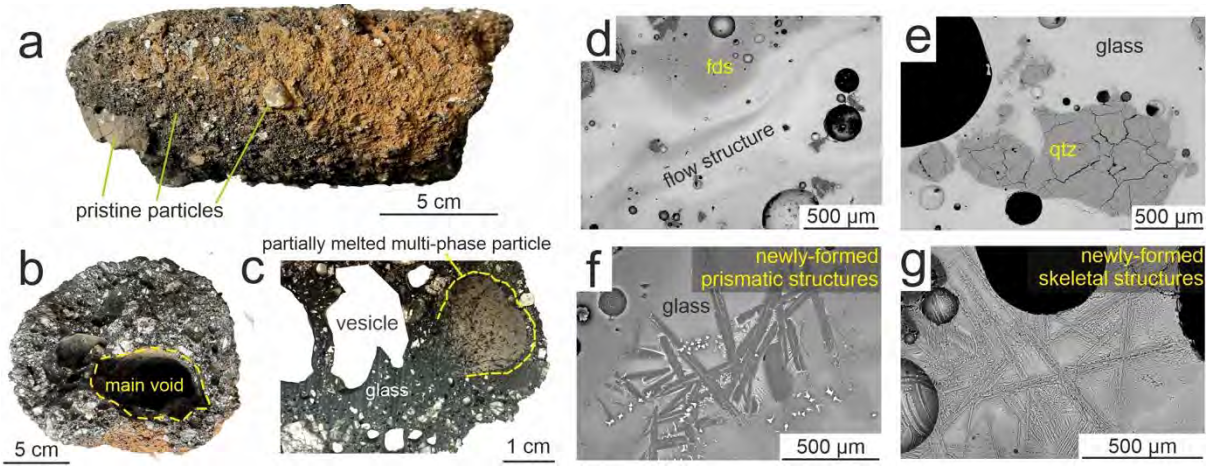

489

490 **FIGURE 3.** Detailed optical and BSE images of the natural fulgurite. (a) A photo of the studied
491 part of the fulgurite specimen in detail. (b) A section view of the natural fulgurite exhibits the
492 "main void". (c) An optical image of a segment of a section of the natural fulgurite captured
493 by 3D LSCM, showing vesicles of varying sizes and shapes. (d) The heterogeneous glass mass
494 displays a flow structure within the glass mass. (e) BSE images reveal fractured quartz crystals.
495 (f) Newly-formed prismatic-tabular structures exhibit enrichment in SiO_2, Al_2O_3, Na_2O and
496 K_2O. (g) Newly-formed skeletal structures present MgO enrichment. Feldspar: fds.

497

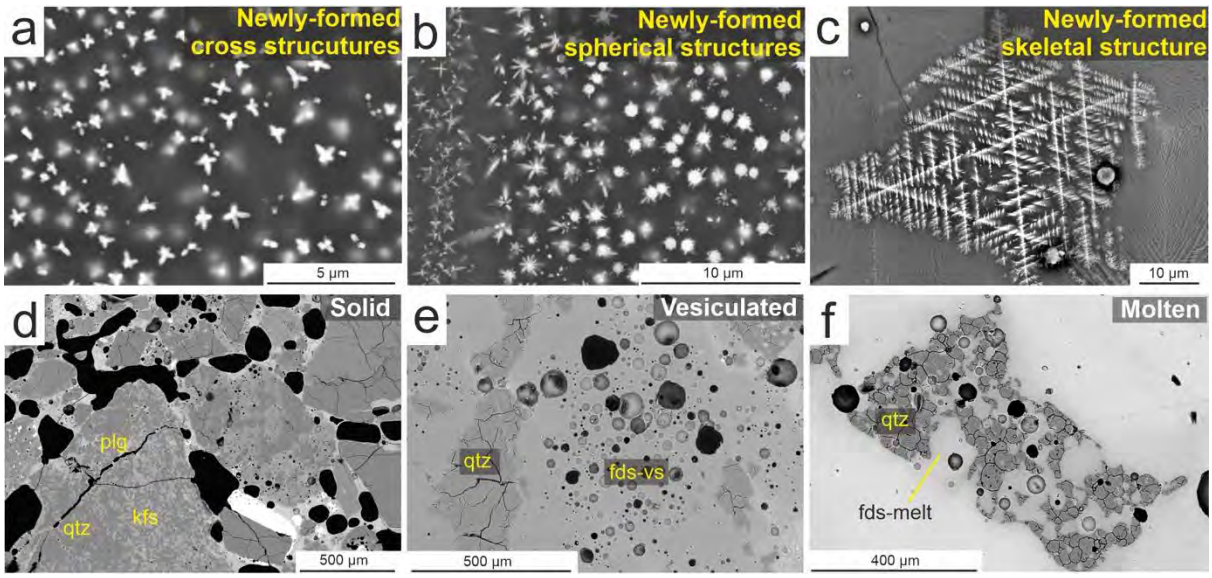

498

499 **FIGURE 4.** Post-melting recrystallization structures and melting morphologies of the main
500 crystals (feldspar) in the natural fulgurite are shown in (a-c) and (d-f), respectively. Fe-rich
501 recrystallization structures grew in different forms, such as cross (a), spherical (b), and skeletal
502 (c). (d) Unmelted polymineralic grains are named “solid”. (e) Feldspar displays vesicles due to
503 high-temperature interactions in the “vesiculated”. (f) The “molten” exhibits complete melting
504 of the feldspar. Vesicle: vs.

505

This is the peer-reviewed, final accepted version for American Mineralogist, published by the Mineralogical Society of America.
The published version is subject to change. Cite as Authors (Year) Title. American Mineralogist, in press.
DOI: https://doi.org/10.2138/am-2023-9192. http://www.minsocam.org/

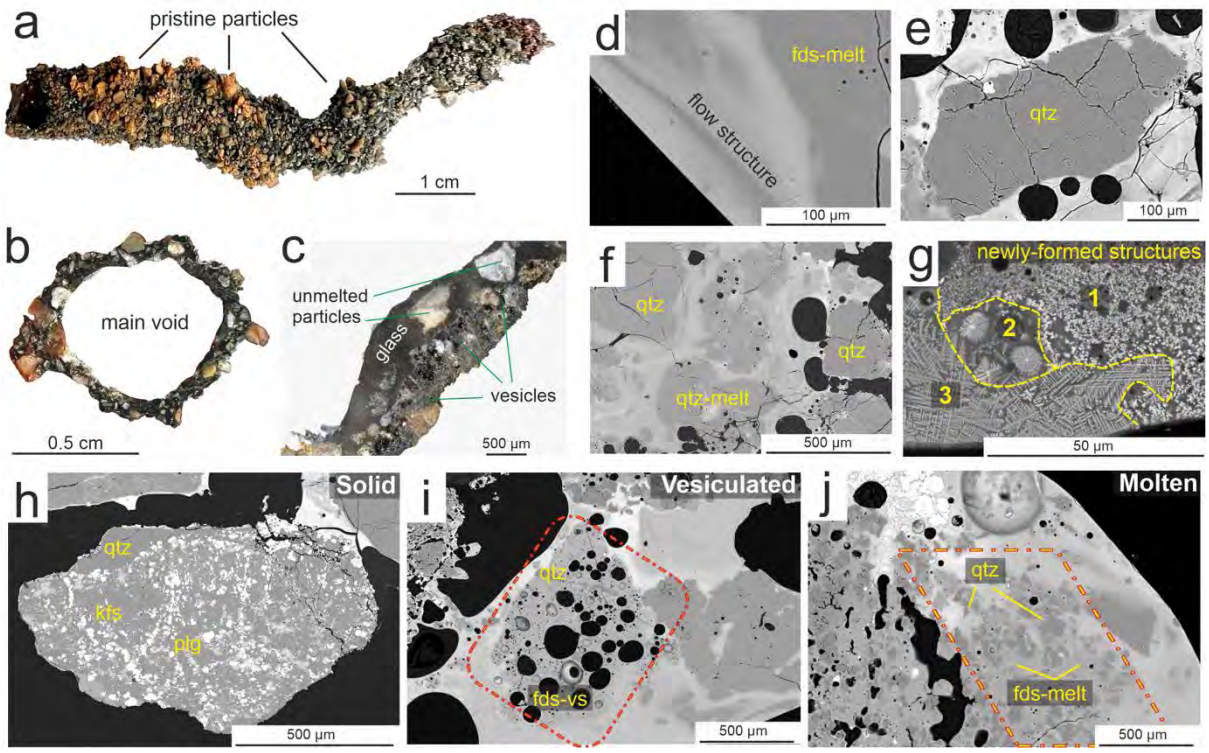

506

507 **FIGURE 5.** Optical and BSE images of the experimental fulgurite. (a) A photo of the
508 experimentally generated fulgurite. (b) A sectional view of the experimental fulgurite. (c) An
509 optical image of the fulgurite shows unmelted and partially-melted mono- and polymineralic
510 grains in a glassy mass. (d) Partially-melted feldspar crystals, which have mingled with the
511 glass mass. (e) A BSE image of a monomineralic partially-melted quartz. (f) Partially-melted
512 quartz and alkali feldspar crystals. (g) Newly formed structures grew in different forms (i.e.,
513 spherical and skeletal). The feldspar crystals exhibit a "solid" (h), "vesiculated" (i), and
514 "molten" morphologies (j) in the polymineralic grains.

515

This is the peer-reviewed, final accepted version for American Mineralogist, published by the Mineralogical Society of America.
The published version is subject to change. Cite as Authors (Year) Title. American Mineralogist, in press.
DOI: https://doi.org/10.2138/am-2023-9192. http://www.minsocam.org/

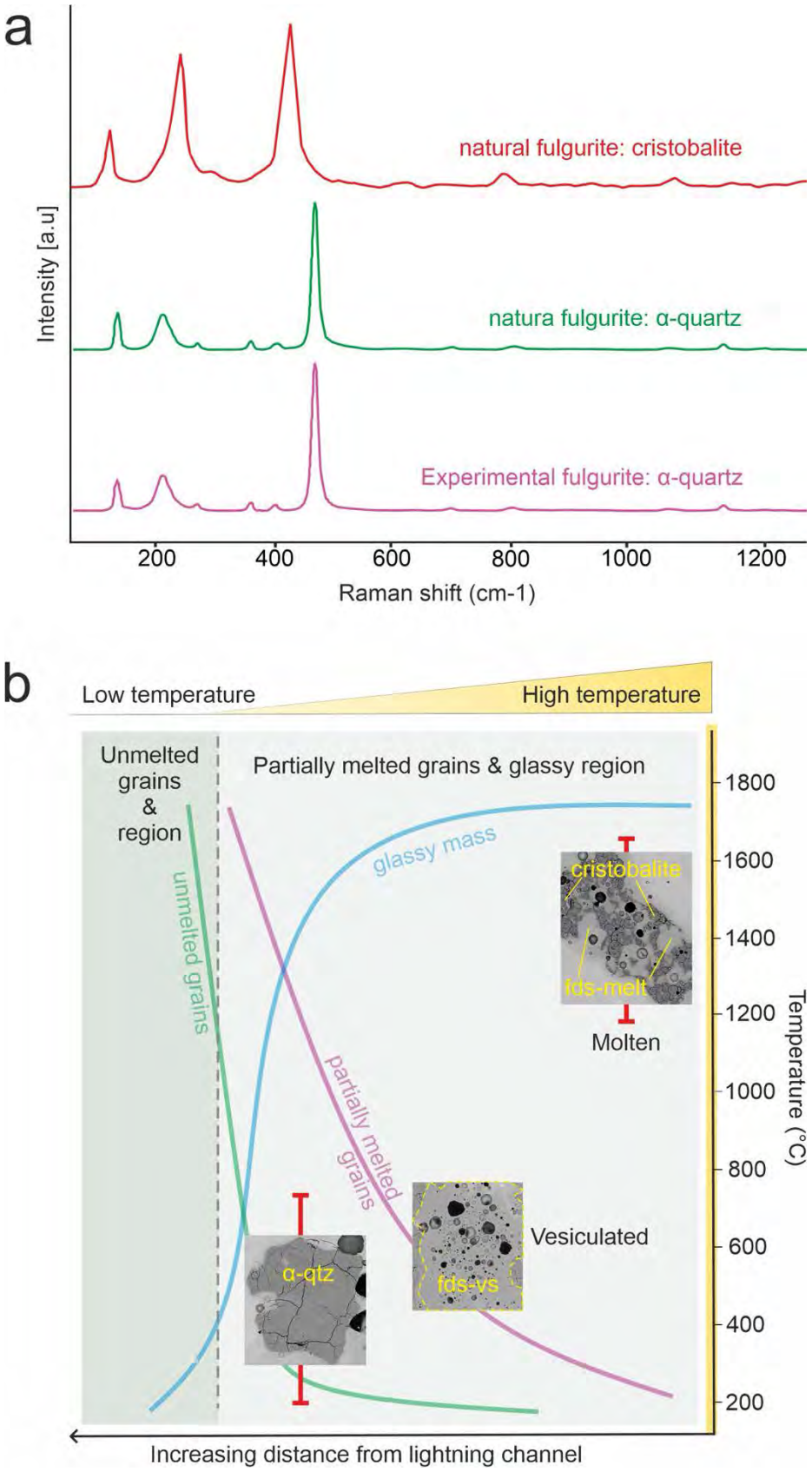

516

517 **FIGURE 6.** Micro-Raman spectroscopy of quartz crystals and a schematic diagram illustrating

518 the evolution of grains in the fulgurites. (a) The Raman spectra of quartz crystals in fulgurites

519 from each fulgurite's inner and outer walls. The experimental fulgurite exhibits only α-quartz
520 and natural fulgurite displays both α-quartz and cristobalite. (b) The textural evolution of the
521 fulgurites concerning temperature development during lightning discharge. The textural
522 evolution among the defined morphologies (i.e., solid, vesiculated, and molten) is scaled in
523 temperature using the α-β transition (Folstad et al., 2023) and cristobalite stability (Wagstaff
524 1969).

525 **TABLE 1:** WWLLN data around the sampling area of the natural fulgurite.

Type of lightning	Date	Time	Location	Peak current [kA]	IC height [km]	Number sensors
IC	01.04.20	12:25:32	38º15'01.2"N 44º18'32.7"E	5.113	18.917	5
CG-1	01.04.20	17:27:14	38º11'04.6"N 44º17'19.3"E	-14.473	0	6
CG-2	01.04.20	17:29:41	38º14'22.2"N 44º16'47.3"E	-11.960	0	5

526

527 **TABLE 2.** Chemical composition of natural and experimental fulgurites (SEM-EDS
528 normalized data).

Natural fulgurite										
		Melting morphologies of feldspar				Post-melting recrystallization structures				
	Glass mass	Solid		Vesiculated	Molten	Fe-rich phases			Prismatic -tabular	Mg-rich skeletal
		Plagioclase	Alkali feldspar			Cross	Spherical	Skeletal		
Si_2O	60.11	66.07	64.69	67.24	69.21	57.31	42.29	3.60	56.89	54.07
Al_2O_3	17.01	21.45	18.82	20.76	17.41	13.50	11.45	2.12	25.94	4.89
FeO	9.91	0.17	0.14	0.19	2.99	22.92	35.21	91.23	2.14	12.76
CaO	3.29	1.85	0.06	0.69	1.95	0.78	0.81	0.01	8.63	2.22
K_2O	2.61	0.96	14.63	3.53	3.30	0.37	0.31	0.02	0.60	0.36
Na_2O	3.09	9.31	1.58	7.35	3.63	2,41	4.16	0.18	5.13	0.56
MgO	2.49	0.1	0.02	0.09	1.20	1.63	2.02	0.50	0.34	24.19
TiO_2	1.26	0.04	0.02	0.03	0.24	1.01	3.15	1.86	0.22	0.47
MnO	0.19	0.02	0.01	0.03	nd	0.05	0.13	0.03	0.04	0.28
Cr_2O_3	0.04	nd	0.02	0.02	nd	0.02	0.02	0.06	0.07	0.02
W	nd	Nd	nd	nd	nd	nd	0.45	0.19	nd	0.09
Cu	nd	0.03	0.01	nd	0.08	nd	nd	0.02	nd	nd

Experimental fulgurite								
		Melting morphologies of feldspar				Post-melting recrystallization structures		
	Glass mass	Solid		Vesiculated	Molten	Fe-rich phases		
		Plagioclase	Alkali feldspar			Structure 1	Structure 2	Structure 3
Si_2O	64.11	65.48	63.77	66.07	63.98	21.53	21.61	42.07
Al_2O_3	17.78	21.87	18.89	19.14	24.42	nd	8.31	14.42
FeO	6.71	0.92	0.24	2.35	0.38	77.13	65.26	31.52
CaO	3.57	0.65	0.07	0.52	0.88	nd	1.26	1.73
K_2O	1.91	1.94	16.68	8.05	2.82	0.07	0.42	1.94
Na_2O	2.28	8.38	0.22	3.27	7.20	1.12	0.80	2.33
MgO	1.52	0.31	0.08	0.5	0.16	nd	1.03	2.78
TiO_2	1.18	0.10	nd	nd	nd	0.04	1.04	2.98
MnO	0.11	0.25	0.02	nd	0.39	nd	0.08	0.20
Cr_2O_3	nd	0.10	nd	nd	0.55	0.10	0.17	nd
W	0.72	0.35	nd	nd	0.06	0.01	nd	nd
Cu	nd	nd	0.03	0.01	0.10	nd	0.04	nd

529